Ultrastructure of Insect and Spider Cocoon Silks

Osnat Hakimi,*,† David P. Knight,‡ Martin M. Knight,† Michael F. Grahn,§ and Pankaj Vadgama†

Interdisciplinary Research Center in Biomedical Materials, Materials Department, and Center for Academic Surgery, Queen Mary University of London, London E1 4NS, and Department of Zoology, University of Oxford, South Parks Road, Oxford OX1 3PS, United Kingdom

Received June 1, 2006; Revised Manuscript Received August 9, 2006

Despite much interest in the extraordinary mechanical properties of silks, the structure of native silk fibers is still not fully understood. In the present study, the morphology, topography, and organization of insect and spider cocoon silks were investigated using a range of imaging methods. Field emission scanning electron microscopy was used to observe transverse and longitude structures in silk fibers subjected to tensile fracturing, freeze fracturing, or polishing. In addition, ultrathin sections of silk brins embedded in resin were examined using transmission electron microscopy. Finally, dry silk brins were examined by confocal microscopy. The results confirmed the existence of well-oriented bundles of nanofibrils in all the silks examined and gave an indication of a hierarchical construction of the brin. Observed separation of the microfibrils in fractured brins suggests that the multifibrillar structure of the silk fiber contributes to toughness by allowing dissipation of energy in the controlled propagation of cracks.

Introduction

While orb web spider dragline silk shows remarkable tensile properties,[1] Mulberry silk shows comparable toughness[2] when artificially drawn from the living silkworm under defined conditions. This has led to attempts to use silk proteins to make tough filaments and a range of nonextruded materials.[3] Given that the extraordinary properties of silks depend on the organization of the fibers, it is unfortunate that the structure of silk threads is still incompletely understood. Surface topography, morphology, and the average diameter of silk filaments have been only partially described in the literature, and there are several conflicting models for the micro- and nanostructure of the natural fibers. In addition, most of the suggested models are for spider dragline silk,[4,5] and there are no specific, comprehensive models for the nano- and microarchitecture of lepidoptera cocoon silks.

The structure of cocoon silks is of interest for a number of reasons. First, a knowledge of the hierarchical structure of silk fibers can better the understanding of the relationship between the molecular structure of component proteins and their assembly and their interaction to define the mechanical properties of silks.[6,7] Second, silk is gaining popularity as a biomaterial for tissue engineering, and as a biomaterial, its structural properties are likely to affect cell morphology, alignment, migration, and metabolism and differentiation of adherent cells.[8]

Several techniques have been used to investigate the structure of silk fibers in previous studies. Light microscopy has been used to examine *Nephila clavipes* dragline silk swollen by treatment with the chaotropic agent urea. This simple technique provided some evidence that the thread core is composed of "twisted bands of microfibrils".[4]

Transmission electron microscopy (TEM) has been used to analyze the structure of major ampullate silk from *Nephila madagascariensis*, showing the presence of a thin outer layer to the fiber (possibly a skin structure), an additional coat, and elongated cavities oriented parallel to the silk fiber axis.[9] The latter are thought to be formed during silk spinning, from small droplets in the stored spinning dope.[10] Similar elongated microvoids have been described in *Bombyx mori* silk filaments and are thought to originate in the same way.[11] However, TEM imaging to date has been limited due to the challenge of infiltrating and cutting good ultrathin sections of the tough fiber, as well as aligning the fibers to achieve transverse and longitudinal cross sections.[12] Small-angle X-ray scattering and atomic force microscopy (AFM) have been used to investigate the morphology of cocoon silk from *B. mori* and dragline silk from *N. clavipes*. AFM imaging provides further evidence for the existence of nanofibrils in silks,[13] while AFM force measurements and the study of Raman shifts produced by stretching silk fibers provide evidence that these nanofibrils may be contributing to the remarkable toughness of silks.[14] AFM, scanning electron microscopy (SEM), and wide-angle X-ray diffraction (WAXD) have also been used to show that various silkworm silks contain nanofibrils.[15] Evidence from NMR and small-angle X-ray scattering gives indication of rather precise orientation of the β-sheets to the long axis of spider dragline fiber.[16,17]

SEM has also been used on fractured surfaces of spider major ampullate and silkworm silks broken in a tensile testing machine. Resulting transverse sections illustrated variation in brin shapes and sizes in *B. mori* and presented further evidence for a nanofibrillar arrangement of all the silks investigated.[18] Despite the use of the range of techniques described here, there are still gaps in the understanding of silk supramolecular structure and assembly.

The aim of the present study was to investigate the morphology, topography, and organization of cocoon silks from the silkworms *B. mori* and *Antheraea pernyii*, as well as egg cocoon

* To whom correspondence should be addressed. E-mail: o.hakimi@qmul.ac.uk. Phone: (+44) 0207 882 5547. Fax: (+44) 0208 983 1799.
† Materials Department, Queen Mary University of London.
‡ University of Oxford.
§ Center for Academic Surgery, Queen Mary University of London.

10.1021/bm060528h CCC: $33.50
Published on Web 09/12/2006

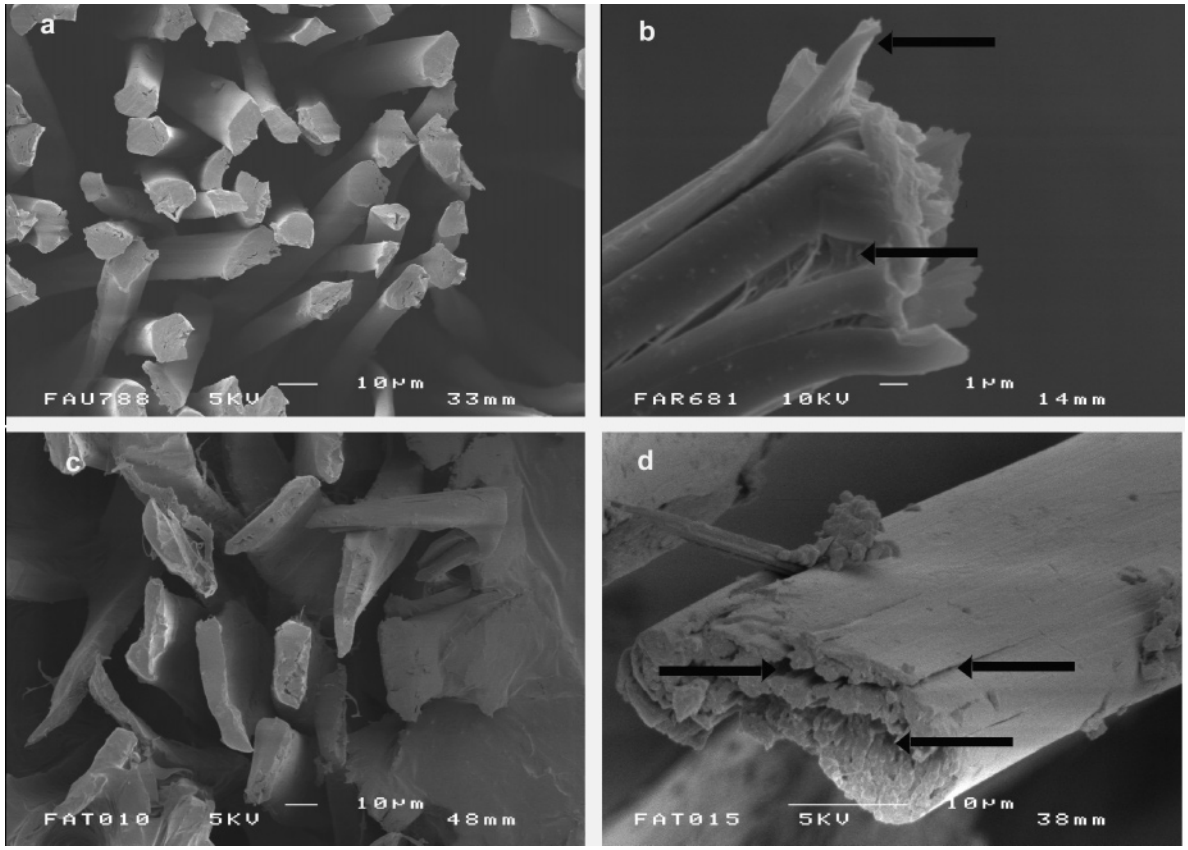

Figure 1. SEM micrographs of transverse fractures of silk brins: (a) *B. mori* and (c) *A. pernyii* fractured in liquid nitrogen, (b) *B. mori* and (d) *A. pernyii* broken during tensile testing. Arrows indicate fractures propagated longitudinally and transverse to the fiber axis, as well as plastic deformation in *B. mori* (b).

silk from the spider *Nephila edulis*, using a range of advanced microscopy methods. Field emission scanning electron microscopy (FE-SEM) was used to observe transverse and longitude structures in silk fibers subjected to tensile fracture, freeze fracture, or polishing. In addition, ultrathin sections of silk brins embedded in resin were examined using TEM. Finally, dry silk brins were examined by confocal microscopy. The results confirmed the existence of well-oriented nanofibrils and gave an indication of a hierarchical construction of the brin.

Materials and Methods

Short staples of combed out and conventionally degummed *B. mori* and *A. pernyii* silk brins were supplied by Gaddum Ltd., U.K. Fully formed *N. edulis* egg sacs (cocoons) were collected from spiders growing in a heated greenhouse (supplied by the Prof. Fritz Vollrath laboratory, Oxford University), and the egg mass was removed manually from the sac.

For mechanical tests, single silk fibers (or brins) were glued using superglue gel (Loctite Ltd.) to cardboard frames. After the cardboard was cut, the brins were tested to failure in screw-driven series 9 Instron 4464 mechanical testing instruments with the following conditions: 2.5 N load cell, crosshead speed of 7.5 mm/min, specimen length 2−3 cm, room temperature (18−20 °C), ambient humidity (approximately 50%). Fibers that failed at a distance greater than 1 mm from the attachment point were mounted on aluminum stubs for SEM fractographic examination.

For freeze fracture, silk fibers were soaked in superglue gel and rolled in thin cardboard (as in a preparation of a cigarette) to form a dense, filled tube. The tubes were allowed to dry at room temperature for 5 min and then dipped in liquid nitrogen for 2 min. Upon removal from liquid nitrogen, the tubes were quickly sliced using a clean razor blade and the sliced tubes mounted on aluminum stubs.

For the polishing of silk brins in resin, random meshes of brins/silk fibers in 25 mm diameter moulds were covered with a resin mixture of Epofix resin with 15% hardener (Struers, Scotland) and vacuum embedded (Epovac vacuum embedders, Logitech, Scotland). The resin was left to polymerize for at least 16 h at room temperature. The embedded samples were then ground and polished using diamond pads in DP blue (alcohol-based lubricant, Struers). The samples were desiccated overnight and then coated with a conductive gold layer using a Balzer sputter coater. They were examined in a JEOL 6300 F field emission scanning electron microscope (JEOL UK Ltd.) with an accelerating voltage of 5 or 10 kV.

For TEM, meshes of the different silk types were separately fixed in 2.5% glutaraldehyde in 0.1 M cacodylate buffer (1.5 h, 20 °C), washed in cacodylate buffer, and post fixed for 1 h in aqueous nonbuffered 1% osmium tetroxide. After dehydration in a methanol series, the samples were treated with 1,2-propylene oxide and infiltrated overnight in a 50:50 mixture of propylene oxide and resin (TAAB Laboratory Equipment Ltd., Berkshire, England). The resin concentration was then increased every 3−4 h by removing 1 mL of the resin/propylene oxide mixture and replacing it by 1 mL of pure resin. After three such increases, the samples were placed in pure resin for at least 12 h, followed by a final change of pure resin before curing in an oven at 60 °C for at least 48 h.

Ultrathin sections were cut with a diamond knife. The sections were approximately 60−70 nm thick as judged by their interference colors and were collected on bare copper grids. The sections were stained in 1% alcoholic uranyl acetate and lead citrate as a nonspecific stain. The sections were examined in a JEOL 2010 transmission electron microscope (80 kV). Low beam intensities were used as high beam intensities caused immediate damage to the sections.

For confocal microscopy, dry, untreated silk brins and fibers were mounted on glass coverslips using standard adhesive tape. Autofluorescence was excited at 633 nm using a Leica confocal microscope

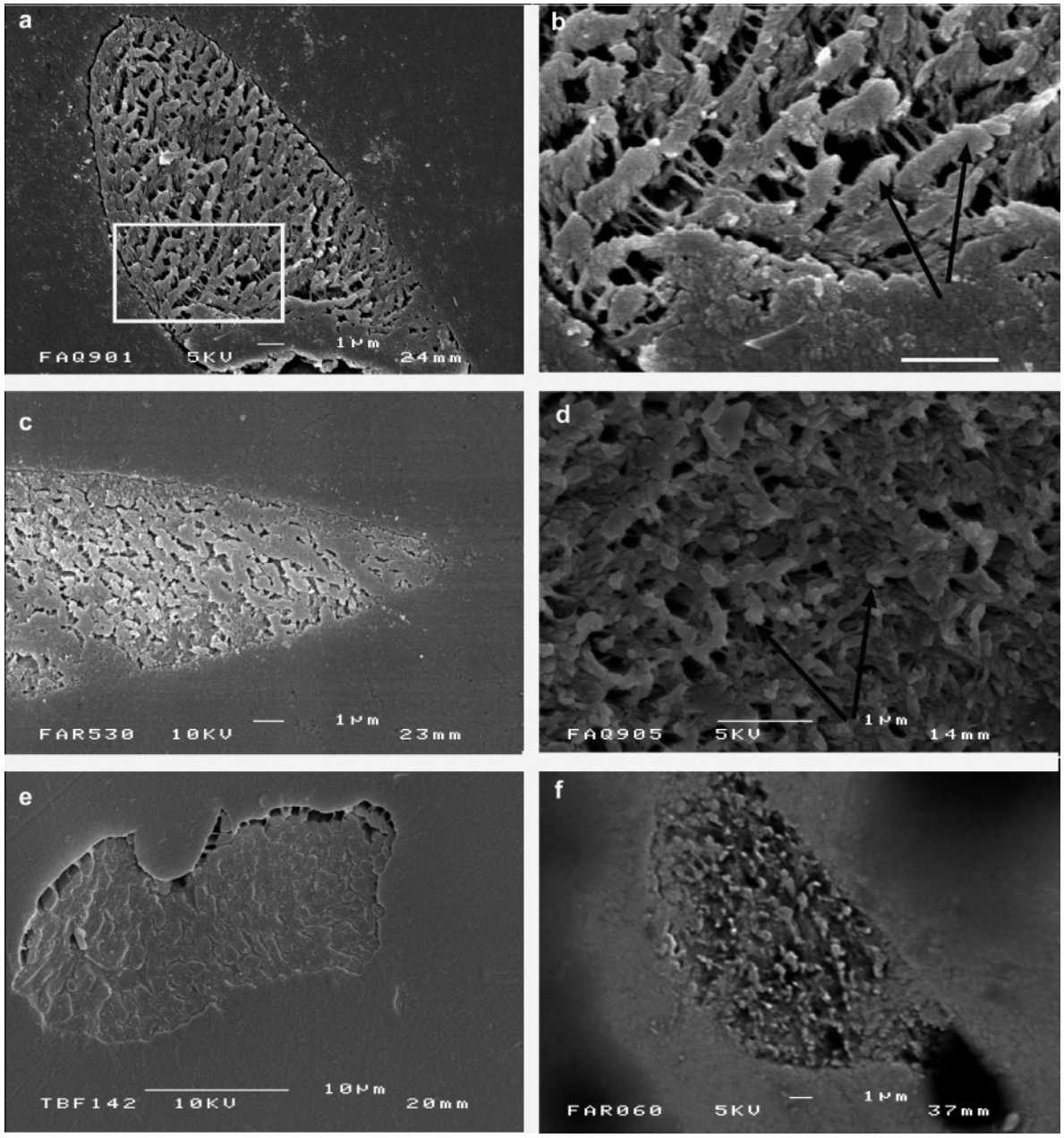

Figure 2. SEM micrographs of transverse cross sections of silk brins produced by epoxy resin embedding and polishing: *B. mori* section (a) and a magnified view of the boxed region (b) (scale bar represents 1 μm), *A. pernyii* (c, d), *N. edulis* (e, f). The arrows in (b) and (d) indicate bundles of nanofibrils or microfibrils.

(TCS SP2 confocal microscope, Leica Microsystems Ltd., with a 63× objective lense). Confocal Z series were obtained throughout the thickness of the thread with a pixel size of 0.1 μm and a *z* step size of 0.2 μm. Emission was detected at 400−600 nm.

Results

Transverse Surfaces. SEM images of *B. mori* and *A. pernyii* transverse-cut brins are presented in Figures 1 and 2, and TEM images are in Figure 3.

SEM imaging of the brin's transverse cross sections (Figures 1 and 2) clearly showed the microfibrillar construction of the thread. Cold-fractured specimens presented in Figure 1a,b showed a fairly clean brittle fracture with no evidence of the plastic deformation observed for *Nephila* dragline fractured in liquid nitrogen.[19] Specimens fractured at room temperature showed a less clean break with cracks running longitudinally some distance down the brin (Figure 1c,d). Some of these cracks may have followed the longitudinal "voids" (canaliculi) seen in silk fibers or lines of weakness between nanofibril bundles. In *A. pernyii*, the cracks appear to propagate both longitudinally and transversely (Figure 1d, arrowed). There is some evidence for plastic deformation in the *B. mori* brin (Figure 1c, arrowed).

B. mori brins, 7−12 μm in diameter, had a roughly circular to elliptical profile, often with a single flattened or slightly concave facet, probably produced during the pressing of two brins into a single fiber by the silkworm.[20] *A. pernyii* fibers were ribbon shaped with a maximum width of 20−30 μm. One surface frequently appeared concave and the other convex, again possibly as a result of partial shaping in the silkworm silk press.

Parts a−f of Figure 2 are images of transverse cross sections achieved by epoxy resin embedding followed by polishing.

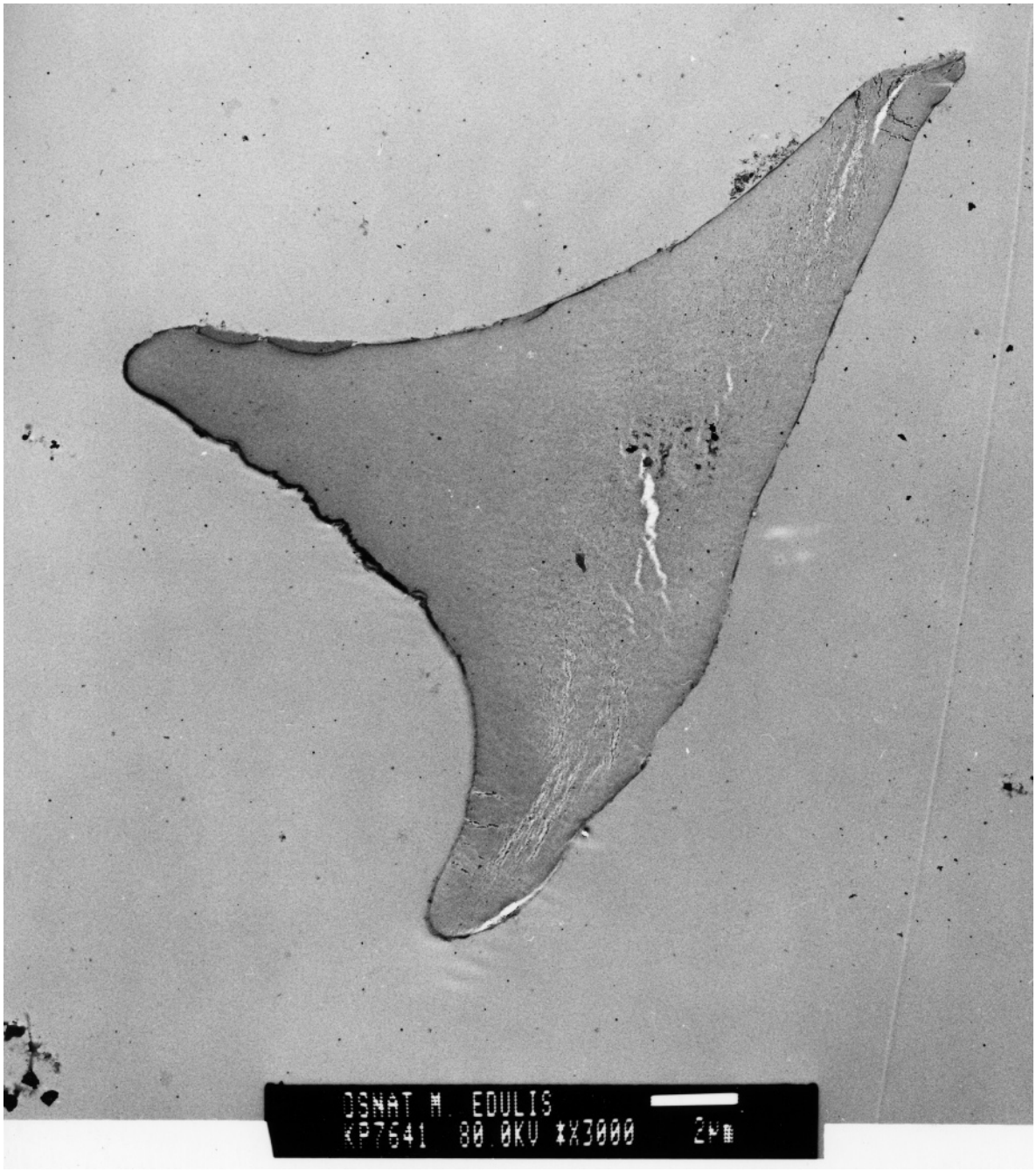

Figure 3. TEM micrographs of transverse cross sections of *N. edulis*. The bar represents 1 μm.

Evidence of nanofibrillar substructure can be seen in the three silks studied. The microfibrils seen in Figure 2b,d may represent "bunches" of nanofibrils possibly clumped during grinding. In Figure 2a there is also some suggestion of skin-core organization, with a rim of denser material around most of the outer part of the brin. However, it is possible that this is an artifact of the increased support from the resin in this region. Figure 2e shows a transverse cross section of what are possibly two adjacent *N. edulis* brins.

Micrographs of the *B. mori* and *A. pernyii* show voids between nanofibrils. These may represent the canaliculi or voids described in *Nephila* dragline silk[9] and *B. mori*,[11] although they are probably too numerous and we cannot completely eliminate the possibility of polishing artifacts, including plastic deformation, cracks, and dents. To overcome this problem, alternative visualization methods were sought, including TEM and confocal microscopy.

Figure 3 is a TEM micrograph of *N. edulis* cocoon silk transverse ultrathin sections. It clearly shows the three-armed appearance observed in the cocoon silk, possibly formed during extrusion through the cylindriform gland spigots which have a star-shaped opening (D. P. Knight, unpublished results).

Longitudinal Surfaces. SEM micrographs presented in Figure 4 show longitudinal surfaces of brins revealed by embedding and polishing and longitudinal views produced by fracturing at room temperature. Although micrographs of tensile-tested fibers provide little additional structural information, they appear to confirm the nanofibrillar nature of all silks tested. Figure 4f shows *N. edulis* cocoon silk fractured on the Instron.

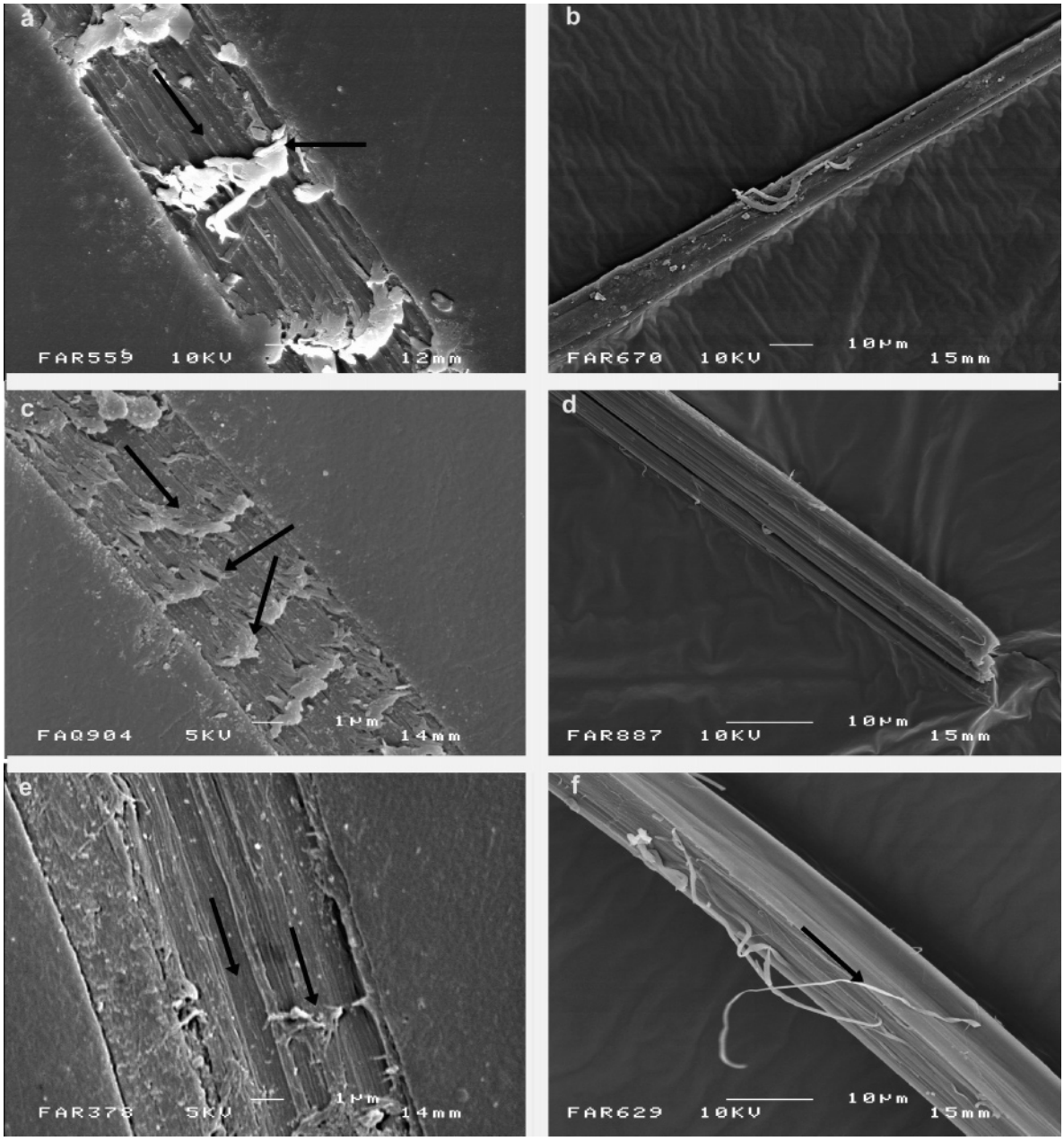

Figure 4. Longitudinal surfaces of silk brins exposed by either polishing, (a) *B. mori*, (c) *A. pernyii*, (e) *N. edulis*, or whole-brin fracture at room temperature, (b) *B. mori*, (d) *A. pernyii*, (f) *N. edulis.* The arrows indicate the orientation of the microfibrils, the possible layered arrangement of the fibers (a, c), and delamination of nanofibrils (f).

The differences between the smooth, relatively patternless appearance of the surface of the thread (on the right side) and the clear fibrillar layout of the inner area of the thread can be seen. This could arise from a surface coating or from a skin-core substructure with more densely packed fibrils in the skin. In addition, delamination of nanofibrils is also evident in this micrograph.

Micrographs of the polished brins suggest a hierarchical construction (especially clear in Figure 4a) of tightly packed nanofibrils assembled to form closely packed microfibrils, with some longitudinally oriented voids or cracks between them. Where the preparation procedure has not disordered the orientation, both nano- and microfibrils appear very accurately aligned along the long axis of the fibril (arrowed in Figure 4a,c,e,f). Parts a and c of Figure 4 also suggest that those microfibrils may be arranged in layers, but the appearance here could be an artifact of polishing similar to the chatter sometimes seen in longitudinal EM sections. Figure 4e shows a nonfibrillar material running in parallel to an *N. edulis* silk fiber, which appears to be much thicker on one side of the thread than the other. This appearance may arise from an uneven coating of gum.

TEM micrographs of transverse sections of *A. pernyii* (Figure 5) show elongated lens-shaped areas oriented parallel to the axis of the thread. These areas have a low but definite electron density and lie between areas of higher density thought to represent nanofibrillar areas. Parts c−e of Figure 5 show that the area closest to the surface of the thread contains fewer of these lens-shaped structures and may represent the skin of the skin-core construction. In some sections (Figure 5a) the lens-shaped structures appeared to have greatly increased in size as a result sectioning damage and/or beam irradiation. These structures are not artifacts as they can also be seen in brins mounted directly in immersion oil and viewed in the differential interference microscope. The tendency of the fiber to split along them may suggest a role in energy dissipation and toughening of the fiber. TEM images of *A. pernyii*, especially Figure 5c,

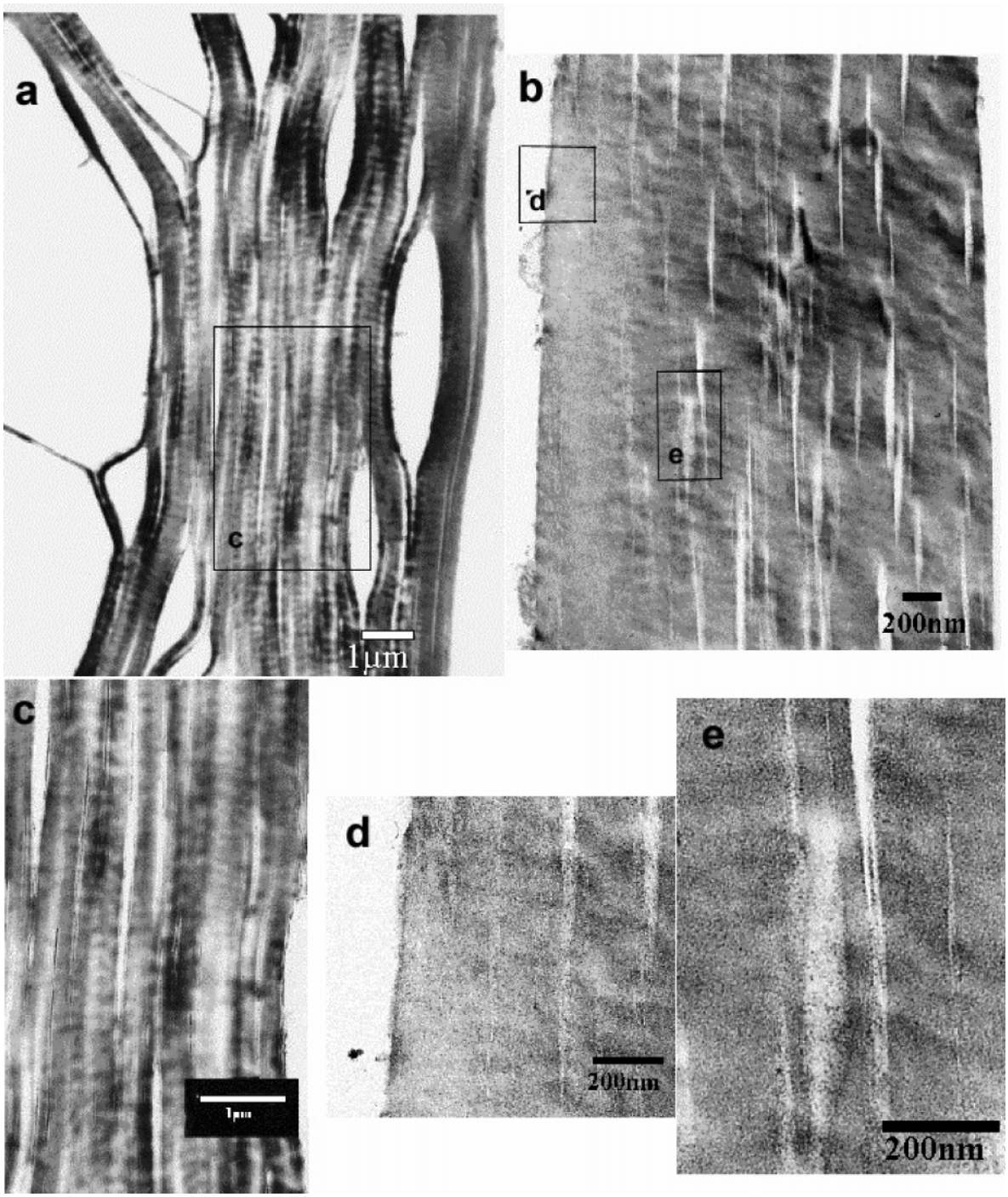

Figure 5. TEM micrographs of longitudinal ultrathin cross sections of *A. pernyii* brins. Magnified regions of (a) and (b) are shown in (c)−(e), as indicated.

appear remarkably similar to micrographs published by Frische et al.[9] of *N. madagascariensis* major ampullate silks.

The short, white lines perpendicular to the axis of the thread (Figure 5a) are probably sectioning artifacts.

Confocal Microscopy. *B. mori* and *A. pernyii* cocoon silks exhibited weak autofluorescence at 633 nm excitation using conventional confocal microscopy. *A. pernyii* showed sufficient autofluorescence to allow visualization of a microfibrillar texture. Figure 6 shows a typical Z series of an *A. pernyii* section, approximately perpendicular to the brin axis. The fibrillar arrangement of the silk can be clearly seen, with fibrils oriented fairly accurately along the axis of the thread. Some fibrils in this series can be followed for the entire length of the frame (see the arrows in Figure 6). Some evidence of elongated, lens-shaped, nonfluorescent areas can also be seen in this Z series (Figure 6), and at least some of these are wide enough to represent the elongated voids previously described in other silks.[9,11]

Discussion and Conclusions

A range of microscopy methods, including SEM, TEM, and confocal microscopy, have been used here to investigate the structure of three cocoon silks: those of *B. mori*, *A. pernyii*, and *N. edulis*. Transverse sections of the three silks studied revealed a microfibrillar substructure. These findings are in line

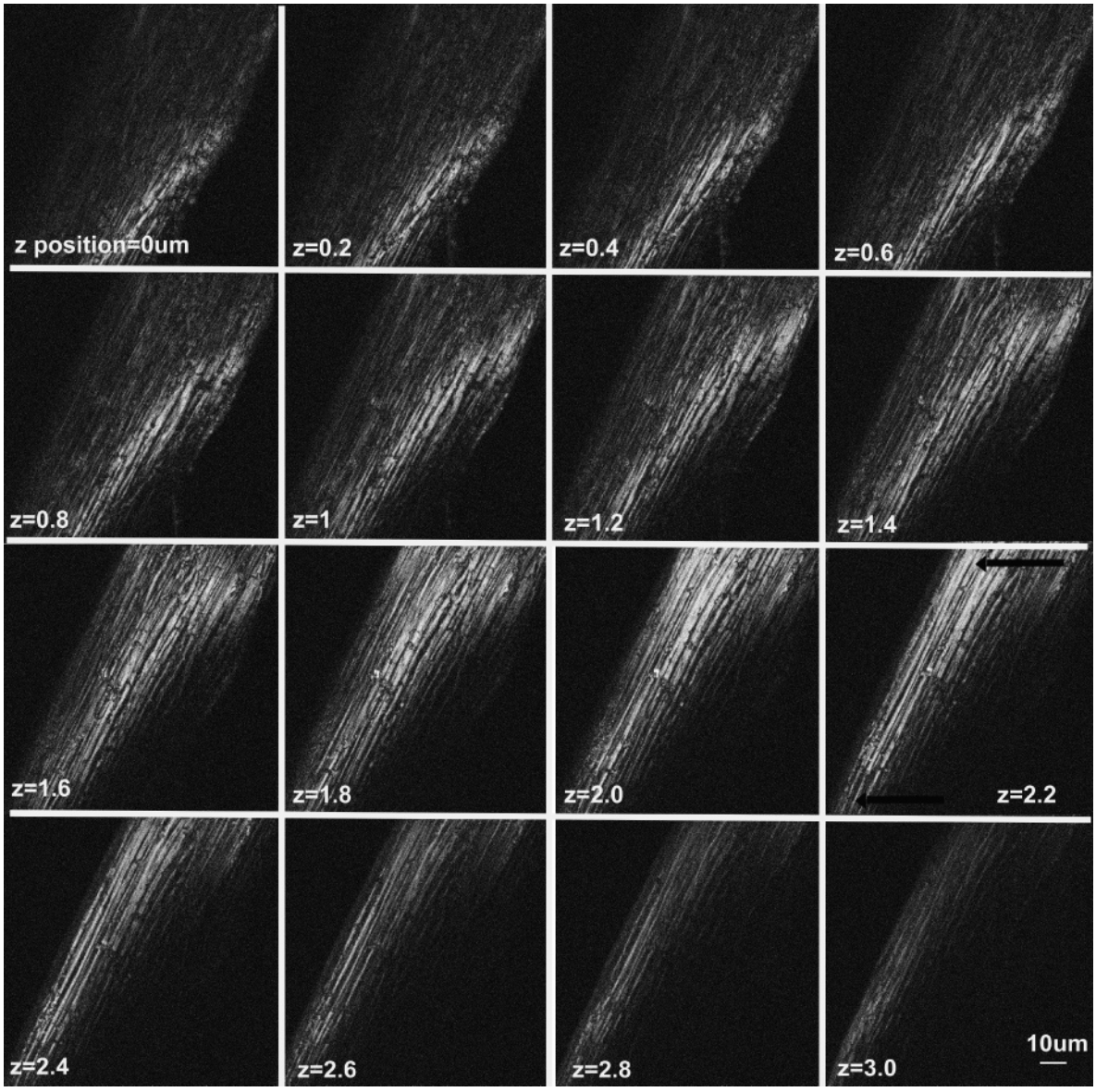

Figure 6. Confocal Z series made through the *A. pernyii* spectrum with a *z* step size of 0.2 μm. The scale bar represents 10 μm. Arrows indicate a microfibril at least as long as the length of the frame.

with those of Poza et al.,[18] who described "bundles of nanofibrils" for *B. mori* and a microfibrillar arrangement in major ampullate silk from the spider *Argiope trifasciata*. In addition, some indication of the skin-core structure could be seen, but further work on this is needed.

Views along the fiber axis confirmed the microfibrillar architecture and clearly demonstrated a nanofibrillar substructure in all three silks. In all silks studied microfibrils were arranged rather accurately parallel to the axis of the thread. The elongated structures described elsewhere as "canaliculi" also appeared to be accurately oriented along the long axis of the brins. Some SEM images showed additional evidence of skin-core organization for *A. pernyii* and *N. edulis*.

Observed separation of the microfibrils and delamination of nanofibrils in tensile-tested brins suggests that the multifibrillar structure of the silk fiber contributes to toughness by allowing dissipation of energy in propagation of cracks. It may also contribute to fiber bending.[15,20] Stress/strain curves of all three silks (not shown here) demonstrated that they ruptured abruptly and completely with no indication of yield or partial shedding of stress. This is compatible with the appearances of the fractured surfaces, which showed little or no evidence of plastic deformation. Also, stress/strain plots showed no events, which could be related to the observed longitudinal crack propagation, but the sampling frequency of the Instron would be insufficient to detect cracking if it occurred just before rupture.

Confocal and field emission gun scanning electron microscopy (FEG-SEM) provided evidence for the absence of helical or obliquely oriented microfibrils in *A. pernyii*, *B. mori*, and *N. edulis* cocoon silks.[4] This absence of oblique microfibrils is in line with findings from wide-angle X-ray microdiffraction[17] as well as Raman shifts and Raman dichroism.[14]

It is possible that specimen preparation for FEG-SEM and TEM had an impact on the ultrastructure of the silk. As pointed out above, artifacts could possibly include plastic deformation, cracks, and dents introduced during polishing and grinding of the resin samples. Although resin is not expected to affect the protein structure or fiber organization, uneven infiltration of the fiber could introduce artifacts such as the skin-core effect observed in some images. Additionally, methanol treatment used here to dehydrate brins has previously been reported to promote changes in the protein secondary structure of silk proteins.[21] Therefore, the conspicuous advantage of using a confocal microscope is the ability to visualize the three-dimensional

ultrastructure of silk fibers in the absence of artifacts associated with specimen preparation. The confocal images presented above confirm at least some of the features observed in SEM and TEM micrographs, such as the well orientated, tightly packed microfibrils in *A. pernyii*. Unfortunately, *B. mori* and *N. edulis* threads do not show sufficient autofluorescence for imaging with confocal microscopy.

Another significant finding from longitudinal FE-SEM views and confocal microscopy was the high packing fraction of microfibrils in the fiber. This, together with their nanofibrillar construction and rather precise longitudinal orientation and the existence of elongated voids with a tendency to propagate cracks, is likely to be important in relating the hierarchical structure of silks to their remarkable tensile properties.

Acknowledgment. This work was supported by the sixth framework program of the European Commission. We thank Professor Fritz Vollrath for the supply of spider egg sac silk and Charlie Campion and Keith Pell for their technical assistance.

References and Notes

(1) Gosline, J. M.; et al. The mechanical design of spider silks: from fibroin sequence to mechanical function. *J. Exp. Biol.* **1999**, *202* (Part 23), 3295−3303.
(2) Shao, Z.; Vollrath, F. Surprising strength of silkworm silk. *Nature* **2002**, *418* (6899), 741.
(3) Nazarov, R.; Jin, H. J.; Kaplan, D. L. Porous 3-D scaffolds from regenerated silk fibroin. *Biomacromolecules* **2004**, *5* (3), 718−726.
(4) Vollrath, F.; et al. Structural organisation of spider silk. *Proc. R. Soc. London, B* **1996**, *263*, 147−151.
(5) Termonia, Y. Molecular modeling of spider silk elasticity. *Macromolecules* **1994**, *27*, 7378−7381.
(6) Hayashi, C. Y.; Shipley, N. H.; Lewis, R. V. Hypotheses that correlate the sequence, structure, and mechanical properties of spider silk proteins. *Int. J. Biol. Macromol.* **1999**, *24* (2−3), 271−275.
(7) Knight, D. P.; Vollrath, F. Biological liquid crystal elastomers. *Philos. Trans. R. Soc. London, B* **2002**, *357* (1418), 155−163.
(8) Altman, G. H.; et al. Silk-based biomaterials. *Biomaterials* **2003**, *24* (3), 401−416.
(9) Frische; Maunsbach; Vollrath, F. Elongate cavities and skin-core structure in *Nephila* spider silk observed by electron microscopy. *J. Microsc.* **1998**, *189* (1), 64−70.
(10) Knight, D. P.; Vollrath, F. Comparison of the spinning of selachian egg case ply sheets and orb web spider dragline filaments. *Biomacromolecules* **2001**, *2* (2), 323−334.
(11) Robson, R. M. Microvoids in *Bombyx mori* silk. An electron microscope study. *Int. J. Biol. Macromol.* **1999**, *24* (2−3), 145−150.
(12) Trancik, J. E.; et al. A simple method for orienting silk and other flexible fibres in transmission electron microscopy specimens. *J. Microsc.* **2001**, *203* (Part 3), 235−238.
(13) Miller, L. D.; et al. Investigation of the nanofibrillar morphology in silk fibers by small angle X-ray scattering and atomic force microscopy. *Int. J. Biol. Macromol.* **1999**, *24* (2−3), 159−165.
(14) Sirichaisit, J.; et al. Analysis of structure/property relationships in silkworm (*Bombyx mori*) and spider dragline (*Nephila edulis*) silks using Raman spectroscopy. *Biomacromolecules* **2003**, *4*, 387−394.
(15) Putthanarat, S.; et al. Investigation of the nanofibrils of silk fibers. *Polymer* **2000**, *41*, 7735−7747.
(16) Hronska, M.; et al. NMR characterization of native liquid spider dragline silk from *Nephila edulis*. *Biomacromolecules* **2004**, *5* (3), 834−839.
(17) Riekel, C.; Vollrath, F. Spider silk fibre extrusion: combined wide- and small-angle X-ray microdiffraction experiments. *Int. J. Biol. Macromol.* **2001**, *29* (3), 203−210.
(18) Poza, P.; et al. Fractographic analysis of silkworm and spider silk. *Eng. Fract. Mech.* **2002**, *69*, 1035−1048.
(19) Yang, Y.; et al. Toughness of spider silk at high and low temperatures. *Adv. Mater.* **2005**, *17* (1), 84−88.
(20) Vollrath, F.; Knight, D. P. Liquid crystalline spinning of spider silk. *Nature* **2001**, *410* (6828), 541−548.
(21) Yang, M.; et al. Structure of model peptides based on *Nephila clavipes* dragline silk spidroin (MaSp1) studied by 13C cross polarization/magic angle spinning NMR. *Biomacromolecules* **2005**, *6* (6), 3220−3226.

BM060528H